RECENT ADVANCEMENTS IN NANOSCALE MATERIALS FROM BIOMASS WASTE DEMONSTRATE EFFICACY IN REMOVING HEAVY METAL IONS FROM WATER

UDC:628.316.12
Original scientific paper https://doi.org/10.46793/adeletters.2025.4.2.1

Mohamed Farouz[1*], Mohamed Okil[1], Ayman M. Mostafa[2], Mohamed M ElFaham[1]

[1]Basic Engineering Sciences Department, Benha Faculty of Engineering, Benha University, Egypt
[2]Department of Physics, College of Science, Qassim University, Buraidah, Qassim City, 51452, Saudi Arabia

Abstract:
High concentrations of heavy metal ions pose several risks to aquatic habitats, primarily from industrial manufacturing and agricultural activities. Some metals, like $Fe^{2+}$and Ni^{2+}, are known to be hazardous to human health if taken internally or inhaled. This work covalently grafted pomegranate peel nanoparticles (PGNS), a green adsorbent with a size of about 45-60 nm, for removing heavy metals from water. The PGNS was analyzed using zeta size and zeta potential determination, field-emission scanning electron microscopy (FESEM), high-resolution transmission electron microscopy (HRTEM), energy-dispersive X-ray analysis (EDXA), Brunauer-Emmet-Teller (BET) surface morphology, and X-ray diffraction (XRD). The study also showed that through the development of PGNS, the surface area of the peel increased by 0.5163 m^2 and the pore diameter by 11.8409 nm compared to raw pomegranate peel (PG). The adsorption efficiency of the synthesized material, PGNS, was studied for removing Fe^{2+} and Ni^{2+} from aqueous media. The outcomes showed that the PGNS obtained high removal efficiencies of 85% for Fe^{2+} and 83% for Ni^{2+} compared to raw PG biomass. The study presents PGNS as a feasible and efficient technology for heavy metal removal and indicates the prospects of developing it as an efficient approach to solving problems of agricultural waste management and water pollution. The research emphasizes that the adsorbent derived from pomegranate peel is effective in treating wastewater, as it is economical, environmentally friendly, and easy to manufacture, due to its simple and benign synthesis methods.

ARTICLE HISTORY
Received: 6 April 2025
Revised: 15 May 2025
Accepted: 2 June 2025
Published: 30 June 2025

KEYWORDS
Eco-friendly nanomaterial, Pomegranate peel, Pomegranate peel nanoparticles, Water treatment, Agricultural waste, Water pollution

1. INTRODUCTION

Water pollution, particularly by heavy industries and manufacturing processes, is a rather tricky problem that requires a solution. The inefficient water supply and demand, coupled with poor water management systems and prolonged droughts, have resulted in a severely limited availability of clean water. These challenges have worsened due to the accumulation of wastewater [1,2]. The entry of one or more thermal, organic, inorganic, and biological pollutants into water leads to deterioration in water quality, posing particular risks to both the environment and human health. More specifically, inorganic pollutants are hazardous because they hardly degrade in the environment, especially metallic inorganic pollutants such as Iron and nickel, which are highly toxic [3]. To address these major and minor issues, it is essential to create and implement comprehensive policies and measures that help mitigate the negative impact on the environment and people's well-being. Heavy metals are introduced into ecosystems due to industrial

*CONTACT: Mohamed Farouz, e-mail: mohamed.abdelaleem18@beng.bu.edu.eg

activities and, more broadly, human activities that deposit these metals into water bodies and soils [4]. It is especially relevant in the developing world because the damage caused by untreated sewage to the environment when discharged into natural water bodies is not well understood. Contamination may severely affect aquatic life and is highly hazardous to human health. It results in deadly chronic diseases, cancers, and neurological diseases, which is ideal when concentrations surpass strictly set limits [5,6]. Therefore, the concentration of heavy metals has become of significant interest in environmental studies, leading to strict policies regarding the amount allowed in drinking water to avoid adverse health and ecological effects. It is now essential to develop concerted measures to solve these pressing issues, develop practical and efficient methods for managing waste, and raise awareness of the importance of preserving clean water sources for future generations. Many new techniques have been designed to remove heavy metals from water supplies significantly. One of them is the use of magnetic Prussian blue (MPB), which is a synthesized sorbent with a very high affinity for the removal of heavy metal ions, namely Cu^{2+}, Co^{2+}, and Pb^{2+}, from aqueous solutions [7-9]. However, some existing water treatment innovations are recent nanotechnology improvements in adsorbent material, photocatalysts, microbial disinfection, and high membrane technology. However, the effectiveness of sieved and coarse sand containing high iron oxide has been observed as an efficient filtration medium on a large scale in aqueous systems for residual organic pollutants and heavy metals [10,11]. The study differs from the rest and can be hailed as a success by providing a green nanomaterial derived from pomegranate peel via inexpensive, direct, and rapid techniques that can support the advancement of water treatment techniques. This study primarily focuses on utilizing biomass derived from PG age using its raw biomass and nanoparticle form to remove Fe^{2+} and Ni^{2+} ions while considering various experimental parameters. By fine-tuning these parameters, it is anticipated that the performance and efficiency of the process for removing heavy metals will improve. The successful application of this technique paves the way for future developments, which would involve investigations on varying weight ratios and a more comprehensive range of heavy metals to enhance this innovative method and expand its various applications. Fe(II) and Ni(II) were selected as target heavy metals because they have serious ecological and toxic effects, are frequently detected in industrial effluents, and have poor adsorption due to their high solubility. Fe(II) leads to high concentrations of water discoloration and health complications, while Ni(II) is toxic and a carcinogen. They have documented that both metals are evident in the Nile River in Egypt and are considered a threat to water quality and human health; the origins of the pollution are effluent discharges from industries, agriculture, and cities' wastewater.

2. MATERIALS AND METHODS

2.1 Bio-Sorbent Preparation

PG is well established as a bio-sorbent with high efficacy for removing metal ions, representing a unique approach to managing waste of low economic value. The production process starts with a pre-cleaning step to remove dust and other contaminants from the surface. Subsequently, moisture is removed from the material through drying, creating the appropriate conditions for size reduction. This procedure resonates with the standard processes exercised in synthesis processes. Precautions are taken regarding the sample selection of waste biomass PG to avoid contaminating the organic matter with other materials and pathogens. The samples were dried in a specialized oven for 72 h at 48°C. The dried samples were ground for several cycles with equal intervals to produce homogeneity. The final powder was passed through meshes (No. 18 and 35) to obtain a fine particle size of less than 1 mm, which may be helpful in further studies. Lastly, samples were stored in moisture-free glass collection tubes [12,13].

2.2 Nano Waste Biomass (PGNS) Preparation

The method of obtaining carbon nanoparticles from PG waste includes the combustion method using these organic materials as nano-sponges. This method mixes the PG with the combustion fuel urea (NH_2CONH_2). The synthesis of nanoscale PG encompasses two primary stages: in the first case, it is a procedure for the preparation of PG, and in the second, it is a procedure for the synthesis of nanoscale materials. The first process is explained in the sub-section known as bio-adsorbent preparation and is further enhanced in this section. In the second phase, PG with urea was re-dissolved in distilled water and impregnated at 80°C to form a gel-like structure. Urea, NH_2CONH_2, was added as

a combustion fuel and Nitrogen source to synthesize PGNS. The process of combustion results in the decomposition of urea, giving off gases such as ammonia (NH_3) and carbon dioxide (CO_2). These gases yield a porous nature within the carbonized material bulk and the surface of the carbon mass, improving the adsorptive capacity. Furthermore, nitrogen from urea is also incorporated into the carbon matrix, forming functional groups that contain nitrogen (-NH_2, -C=O) to enhance complexation and electrostatic attraction processes with heavy metal ions. Subsequently, the gel was sintered in an air furnace at 400°C for 10 min at a heating rate of 5°C per minute in a silica crucible [14]. The combustion process begins with gas production and is notably followed by the evaporation of water. Most importantly, the entire combustion cycle occurs within minutes because of the self-sustaining exothermic reaction, which is non-explosive.

2.3 Heavy Metals Solution Preparation

The specific heavy metal concentrations used in this study were 45 mgL^{-1} iron (II) sulfate (Fe_2SO_4) and 35 mgL-1 nickel sulfate ($NiSO_4$) dissolved in distilled water at a pH of 7. The solutions were first adjusted with the hydrochloric solution to standardize and accurately measure the pH levels. 1M to decrease the pH, and NaOH by 0.1M to increase the pH. It is also important to note that the concentrations of the metal ions must be kept as correct as possible during the experiment; hence, all the experiments were performed in glassware. This approach eliminates the possibility of metal ions adsorbing onto the vessel walls, addressing the actual behavior of metal ions in solution. Altering the parameters enhances the precision of determining the interactions and stability of heavy metals in different water matrices [15,16].

2.4 Materials Used

Applying PG biomass and its derived nanoparticles PGNS can be considered a potential direction for several experimental studies with fixed doses of 200 mg. This controlled approach ensures that the data are collected and analyzed similarly across studies. Nonetheless, to increase the utility and impact of this research, further investigations should place less emphasis on biomass and examine the multiplicity of heavy metals at work. Therefore, by changing the amounts applied during the experiments, researchers should be able to determine the most favorable conditions for the various uses of the chemicals. Furthermore, the study of the influences of heavy metals will provide a better understanding of the enhancement of certain levels in desired applications [17]. In addition to enhancing the precision of the experimental procedure, this multifaceted strategy endeavors to maximize application time, thereby improving the relevance and practicality of PGNS across various disciplines. In future research, these variables should be fully incorporated to harness this new biomass resource for environmental impacts and improvements in material properties.

2.5 Materials Characterization

Particle size and zeta potential were meticulously assessed using a Bruker Zetasizer Nano ZS, following a stabilization period at room temperature and subsequent sonication. Morphological features were scrutinized using a Field Emission Scanning Electron Microscope (FESEM, Quattro S, Thermo Scientific). High-resolution transmission electron microscopy (HRTEM, JEOL JEM-2100 at 200 kV) provided additional insights into the structural characteristics of the materials. The crystalline structure and phase identification were conducted using an Empyrean Malvern Analytical system, while the elemental composition was confirmed through Energy Dispersive X-ray Spectroscopy (EDAX) alongside mapping techniques. Nitrogen isotherm measurements were performed at -196°C to determine the specific surface area, employing the Brunauer–Emmett–Teller (BET) method. The BJH (Barrett–Joyner–Halenda) model was utilized to analyze nitrogen desorption data for pore size distribution. In summary, the study evaluation of surface area, pore volume, and pore size using nitrogen adsorption-desorption techniques provided a remarkable understanding of the material characteristics. Such insights improve knowledge of the synthesized materials' behaviors and their possible uses. X-ray diffraction (XRD) analysis covered a 2-Theta range of 5.0° to 85°, utilizing a step size of 0.04° with a Kα wavelength of 1.54060°.

2.6 Adsorption Experiment

In this study, PG and its nanoscale product PGNS, made from waste biomass, determine the adsorption efficiencies of heavy metal ions from the solution. In the experiment, these materials were

shaken and controlled for 400 min at various pH levels, ranging from 1 to 10, using 100 ml solutions containing iron (Fe^{2+}) at a concentration of 49 ppm and nickel (Ni^{2+}) at 38 ppm. All experiments were conducted at room temperature (25 ± 2°C). To verify the process, samples were taken every 10 minutes to analyse the heavy metal removal efficiency using atomic absorption spectroscopy (AAS). To achieve and sustain the optimum pH levels of the solutions, highly accurate HCl and NaOH solutions were used, and the pH of all solutions was measured using a Quimis model Q400AS pH meter. The adsorption capacity of the PG and its nanoscale variant was determined while maintaining a constant biomass concentration of 200 mg for a series of experiments [18]. The adsorption efficiency was estimated from the initial and equilibrium concentrations of the metal ions using Eq. (1). In addition to identifying the possibilities of applying PG and nanoscale PGNS as organic electrodes for heavy metal removal, the systematic approach presented here enables the exploration of new thrusts regarding other waste biomass and their contribution to environmental remediation [19].

$$Adsorption\ efficiency\ = \left((C_i - C_e)/C_i\right) \times 100 \quad (1)$$

The initial and equilibrium concentrations of the metal ions solution (mg/l) are C_i and C_e, respectively.

2.7 Repetition Type and Data Selectivity

The adsorption studies, material characterization, and isotherm/kinetic measurements were performed in triplicate to minimize the experimental error. The triplicate of each measurement was calculated, and the average values were subjected to data analysis and used in the results section only. All data points deviating from the established trend were re-evaluated, and those inconsistent with replicate experiments were excluded from the final analysis. Its effectiveness is in maintaining the statistical validity of the results and avoiding experimental bias.

3. RESULTS AND DISCUSSIONS

3.1 Zeta Size and Zeta Potential

Analysis of the hydrodynamic diameter of nanoparticles measured using the Zetasizer Malvern instrument. It is dispersed in distilled water at a neutral pH of 7. It provides insights into their dynamic behavior and the presence of an electric double layer on their surfaces using dynamic light scattering (DLS) technology. It is crucial to acknowledge that size measurements are influenced by the solvent and pH conditions [20,21]. The hydrodynamic diameter observed for the larger (PG) particles was approximately 5500 nm, consistent with earlier findings. These larger particles display a negative charge with a zeta potential of -12.3 mV, indicating a stable configuration. Conversely, the hydrodynamic diameter of the (PGNS) revealed some aggregation, resulting in an approximate size of 112 nm and a zeta potential of -42.2 mV. These findings underscore the rapid progress of the removal process. Notably, the electrostatic attraction between positively charged heavy metal ions and the negatively charged particles at the surface-active sites of the PG and its nanoparticle samples is evident.

3.2 Field Emission Scanning Electron Microscopy (FESEM)

To study the surface morphology of PG/ PGNS, FESEM (Field Emission Scanning Electron Microscopy) was used. It is a high-resolution imaging technique that provides information about elemental and structural characteristics at magnification up to 300,000 times. It includes information about elemental and structural characteristics at magnification up to 300,000 times. Micrographs are obtained through a computer program at various magnifications, enabling detailed surface morphological studies with greater efficiency. The rugged morphology of the samples has made it challenging to observe grain boundaries using this imaging technique. However, micrographs have shown drastic differences in properties for both types of samples [22,23]. The original morphology of PG at lower and higher magnification, as shown in Figs. 1 (a-b), reveals important information about the structure on the surface. The rugged surface composition of PG provides an advantage for heavy metal absorption because it contains higher cellulose content, while lignin and hemicelluloses are relatively lower. The morphology of PGNS is shown in Figs. 1 (c-d), which seems more suitable for a heavy metal removal study. Uniform holes and micro-cracks can be seen even at the lowest magnification, showing its complex structure. Clumps can also be observed at all levels, providing a clear picture of the surface

and microstructural characterization of the studied samples.

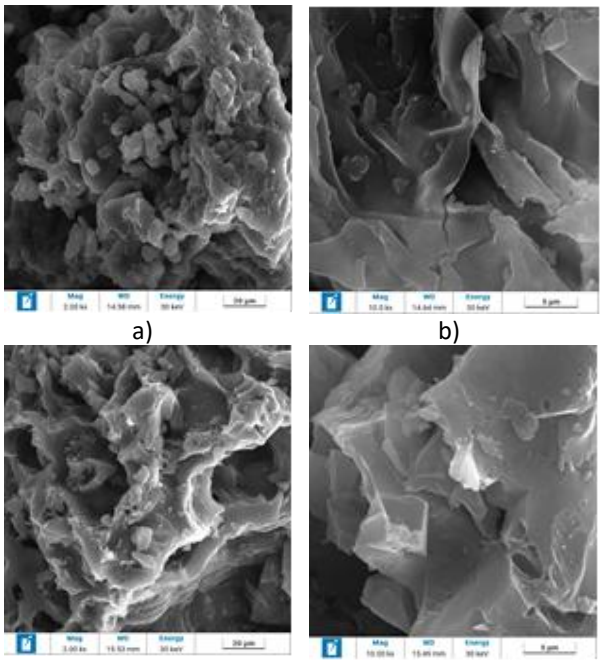

Fig. 1. a-b) FESEM of PG, c-d) FESEM of PGNS

3.3 HRTEM and Selected Area Diffraction (SAED)

HRTEM was conducted to analyze the dimensions and crystallographic characteristics of the PGNS. Figs. 2(a) and 2(b) show that the sulfur nanoparticles are flake-like, as confirmed by the SEM observations. The TEM images depict thin sheet-like structures interspersed with voids measuring between 50 and 70 nm. Fig. 3(b) illustrates the layered architecture of these sheets [24]. On the other hand, Fig. 2(c) displays the HRTEM lattice image with well-defined lattice fringes corresponding to a d-spacing of approximately 0.30 nm. Additionally, as shown in Fig. 2(d), the SAED pattern clearly shows its ring structure, with the d-spacing values included. These calculated d-spacing values enable the assignment of specific hkl values, confirming the successful phase formation for the PGNS. Importantly, these HRTEM results align with those obtained from SEM and XRD studies, enhancing the reliability of the data and the characterization of the nanoparticles under investigation.

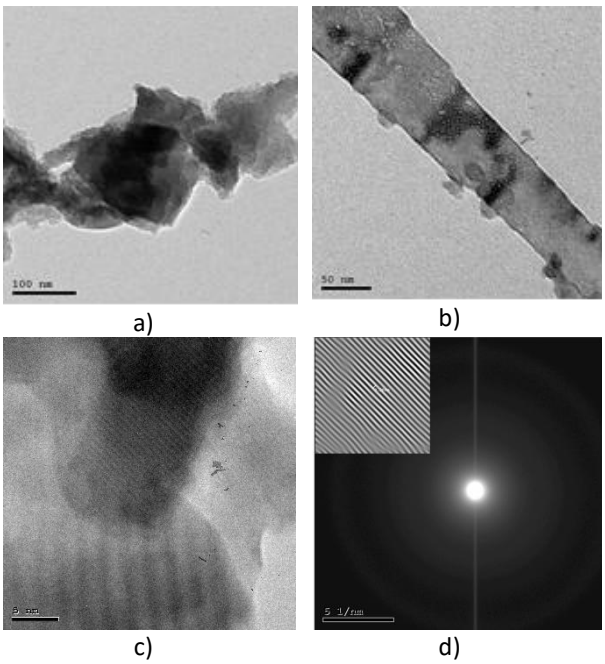

Fig. 2. PGNS a-b) TEM, c) HRTEM, d) SEAD

3.4 Mapping Analysis and Energy-Dispersive X-ray Spectroscopy (EDX)

In a comprehensive analysis of PG and its nanoparticle form, it was identified that distinct elemental compositions comprising Carbon, Oxygen, Potassium, and Calcium in varying proportions [25]. The PG sample exhibited a composition of (64.13%) Carbon (35.49%) Oxygen, with trace amounts of Chlorine (0.07%) and Potassium (0.32%), as illustrated in Figs. 3 (a-b).

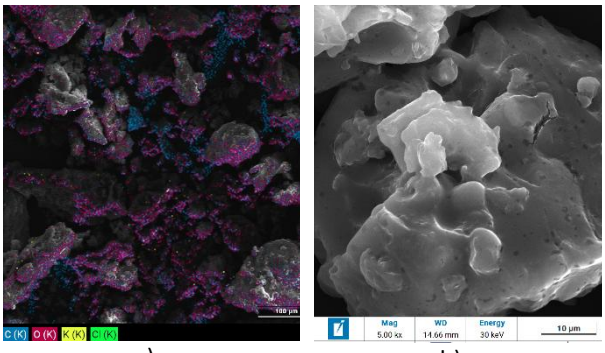

Fig. 3. a) Mapping analysis of the PG, b) SEM of PG

Conversely, the nanoparticle sample revealed a notably higher Carbon content at (83.38%), alongside (15.45%) Oxygen and minor elements, including Sodium (0.24%), Chlorine (0.14%), and Potassium (0.79%), as shown in Figs. 4 (a-b). The detected traces of sodium (Na) in PGNS could be due to the carryover of sodium-containing impurities in the urea used in synthesizing PGNS or residual NaOH from the pH adjustment used in the

adsorption experiments in this research. To accurately determine the adsorption capacity of these critical elements, Energy Dispersive X-ray Spectroscopy (EDX) was utilized, with the findings detailed in Figs. 5 (a-b). Additionally, electron microscopy images, shown in Figs. 3(b) and 4(b) highlighted a significant presence of crystalline grains, indicative of the formation of white minerals within the porous material structure [26]. A summary of the EDX-determined adsorption capacity ratios for the PG and PGNS is provided in Table 1.

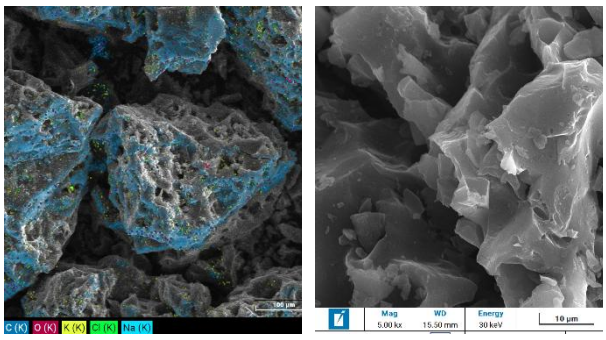

a) b)

Fig. 4. a) Mapping analysis of the PGNS, b) SEM of the PGNS

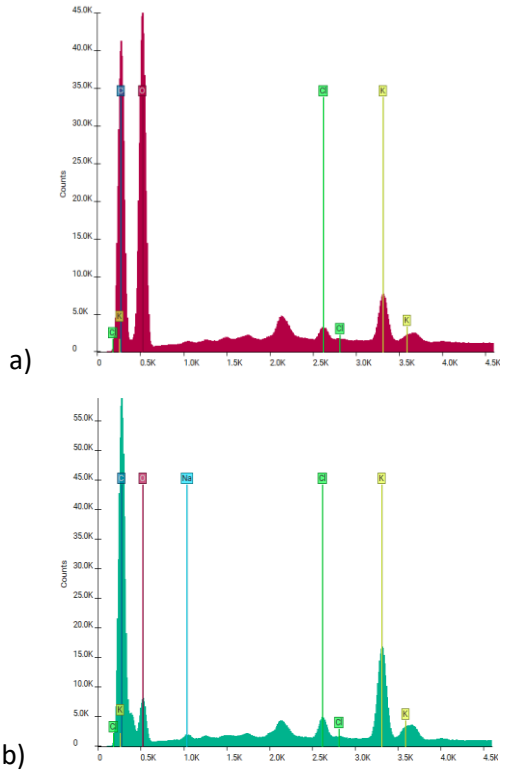

a)

b)

Fig. 5. a) EDX of the PG, b) EDX of the PGNS

Table 1. EDX and mapping data for PG and PGNS samples

Sample	Element	Weight %	Atomic %
PG	Carbon	64.13%	56.93%
	Oxygen	35.49%	41.96%
	Chlorine	0.07%	0.19%
	Potassium	0.32%	0.92%
PGNS	Carbon	83.38%	77.64%
	Oxygen	15.45%	19.17%
	Sodium	0.24%	0.42%
	Chlorine	0.14%	0.39%
	Potassium	0.79%	2.39%

3.5 Brunauer–Emmett–Teller (BET)

The BET analysis indicates that pyrolysis significantly increases the surface area of adsorbent materials. For example, the surface area of PG biomass was initially 0.4219 m^2 but increased to 0.5163 m^2 after pyrolysis PGNS. Additionally, while the average pore diameter of PG was 2.9405 nm, PGNS showed a substantial increase to 11.8409 nm. The BET technique is crucial for defining key parameters, such as mean pore diameter, specific surface area, and overall pore volume, of both PG and PGNS. These parameters are essential for the performance of adsorbents as they determine how the pore architecture interacts with molecules of various sizes and shapes. Accordingly, introducing activation agents could significantly alter the characteristics of PGNS. Studies on surface area and pore characteristics suggest that PGNS could be suitable for adsorbing heavy metals from aqueous environments due to its highly porous nature [27]. Figs. 6 (a-b) illustrate the BET adsorption and desorption, and a comparative methodology was used to analyze the difference between the low-pressure conditions of PG and PGNS. Further discussion will delve into the experimental parameters used and the implications of the findings on performance.

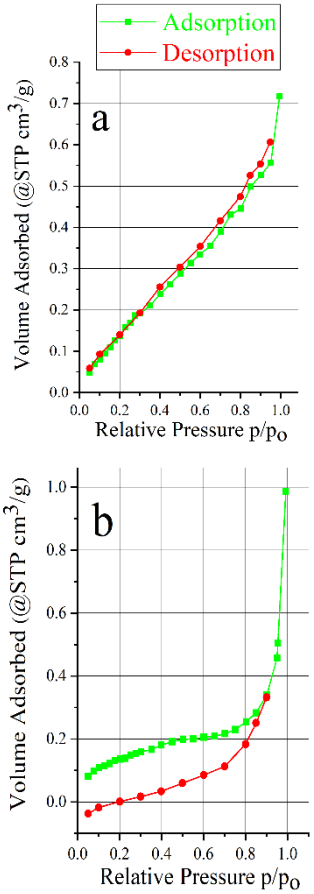

Fig. 6. Nitrogen Adsorption – Desorption analysis a) PG, b) PGNS

3.6 X-Ray Diffraction (XRD)

To examine the crystalline phases of PG before and after its conversion into nanoparticles PGNS, X-ray diffraction (XRD) analysis was performed. The resulting diffraction patterns displayed a variety of crystalline phases, as shown in Figs. 7 (a-b). The XRD analysis of an untreated pomegranate peel sample showed a high correlation with the ICCD standards (00-038-1922), validating the presence of Pyrocatechol ($C_6H_6O_2$) in a monoclinic crystal system. Specific pertinent peaks were noticed on the obtained graph at the following angles: for hkl (-1 1 0) at 18.5°, hkl (-2 1 0) at 22.6°, hkl (3 0 1) at 33.6°, and hkl (2 0 4) at 51.9°. The initial peak had a flattened profile, indicating an amorphous structure in the PG. After thermal treatment, the XRD analysis of PGNS revealed a prominent peak at 25.3°, suggesting enhanced crystallinity of the PG [28,29]. Although a lower-intensity peak was observed, the main structure of the nanoparticles was found to be carbon-based. Additionally, a significant peak was detected at 40.9°. The crystal size was calculated using the Debye-Scherrer (Eq. 2), resulting in a size of 56 nm for PGNS, which contrasts with the original 710 µm size of the PG. This transformation is expected to be crucial for the clearance of heavy metals.

$$d = K\lambda / \beta \cos\theta \quad (2)$$

Here, (d) represents the mean size of ordered crystalline domains, which may be equal to or smaller than the grain or particle size. The shape factor (K), typically slightly more significant than zero and close to unity with a standard value of about 0.9, varies based on the crystallite's geometry. The variable (λ) denotes the X-ray wavelength used in the data analysis. The symbol (β) represents the line width at half the peak height (FWHM), adjusted for instrumental broadening, equal to 2θ. Lastly, (ϑ) indicates the Bragg angle, providing insight into diffraction in crystalline structures. Understanding these parameters will enhance the investigation of crystalline structures.

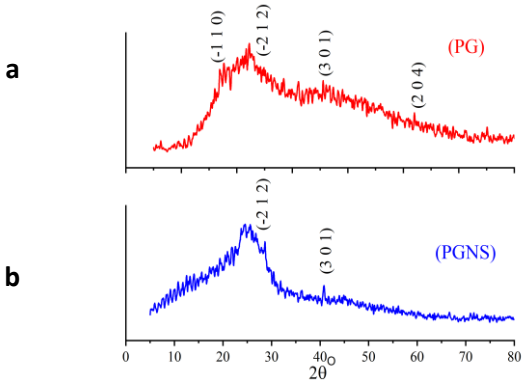

Fig. 7. XRD of a) PG, b) PGNS

3.7 Role of Urea in Modifying PGNS

Urea was blended with PGNS to alter the structure and surface of the material. Results from the BET analysis indicated that the combustion of urea resulted in the formation of a highly porous structure, as the surface area increased from 0.4219 m^2/g PG to 0.5163 m^2/g PGNS. In addition, the nitrogen from urea endowed the PGNS surface with new functionalities, enhancing its adsorption properties Fe^{2+} and Ni^{2+} ions through complexation and electrostatic attractions. These modifications account for the enhanced performance of PGNS over PG in the adsorption analysis.

3.8 Mechanism of Action

Based on the characterization results, possible adsorption mechanisms for PG and PGNS of heavy metal ions (Fe^{2+} and Ni^{2+}) are discussed below. First of all, the zeta potential values of both PG (-12.3 mV)

and PGNS (-42.2 mV) were negative, evidencing that the carboxyl (-COOH) and hydroxyl (-OH) groups contributed to electrostatic interaction with positive metal ions. These findings are underlined by the FESEM and HRTEM data, which demonstrate a highly porous and rough surface morphology of PGNS and thus present many active sites for metal ion adsorption. The BET analysis also reveals the rise in the surface area (0.5163 m^2/g for PGNS compared with 0.4219 m^2 /g for PG) and pore sizes (11.8409 nm for PGNS and 2.9405 nm for PG), which make the adsorption sites more accessible. Also, the XRD result reveals that the thermal treatment enhances the crystallinity of PGNS and may enhance its stability and adsorption properties. The EDX mapping further validates the presence of carbon and oxygen in both PG and PGNS, indicating that these elements are crucial in metal ion adsorption by complexation and ion exchange. In summary, it can be inferred that simultaneous electrostatic attraction, surface complexation, and ion exchange mechanisms are responsible for the high removal efficiency of PGNS because the ion removal efficiencies inferred from this study were Fe^{2+} 85%, and Ni^{2+}83%.

3.9 Assessment of Adsorption Procedure

3.9.1 The Influence of pH on the Efficacy of Fe^{2+} Elimination and Saturation Time Utilizing PG and PGNS

This current investigation established the adsorption capacity of Fe ions using PG and PGNS at a pH range of 1-10 and at room temperature, with a contact time of 40 minutes.

This is depicted by the plots given in Fig. 8, which map the efficiency of the adsorbed sample in each trial against the saturation period. The observed removal efficiency of Fe^{2+} ions was 84.37% when PGNS was used at pH 7, but the removal efficiency was 37.64% in the presence of PG at the same pH (Fig. 8). In the case of PGNS, the saturation time was 190 minutes, while for PG, it was 200 minutes. In particular, the effect of pH on ion removal efficiency is discussed in the work, showing a direct relationship between these factors [30]. The results show a maximum removal efficiency of 37%. It was observed that the highest efficiency of 64% was obtained at a pH of 7 in the solution, and the lowest efficiency was 0.98%. A significant reduction in removal efficiency was seen at pH 1. At pH 10, the removal efficiency for Fe^{2+} using PGNS was reduced to as low as 11% (Table 2). The decrease in adsorption capacity and adsorption rate at high pH can be explained by the adsorption of metal hydroxides such as $Fe(OH)_2$, and an increase in the negative surface charge of the adsorbent may repel metal hydroxide anion species such as $Fe(OH)_3^-$. Additionally, under these conditions, the availability of OH^- ions is relatively high due to the high pH, which hinders the adsorption of Fe^{2+} ions. The maximum time taken to achieve saturation in PG was obtained in 370 minutes, while PGNS acquired better removal efficiencies, recording 83%-47% at pH 7. Nanoparticles exhibited the lowest efficiency at pH 1, reaching only 2%. An efficacy of 11% and a saturation time of 340 minutes were achieved. These results proved the pH dependency of both PG and PGNS in terms of contaminant removal, whereby PGNS displayed a lower saturation time of 190 minutes at the best-selected pH 7.

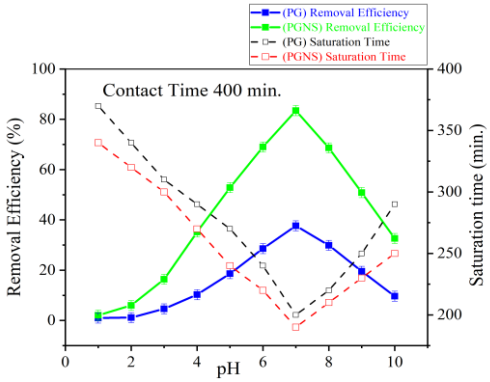

Fig. 8. Fe^{2+} removal efficiency and saturation time of PG and PGNS, error bars represent the standard deviation of triplicate measurements

3.9.2 The Influence of pH on the Efficacy of Ni^{2+} Elimination and Saturation Time Utilizing PG and PGNS

This research builds upon the methodology of the Fe^{2+} elimination experiment, focusing on the adsorption capacity of Ni^{2+} using two materials. Here, PG represents the projection of gain in investing towards the actions indicated in the plan, and PGNS is the gain towards the new state proposed in Eq. 7. A process adsorption study was carried out at a pH range of 1 to 10, at room temperature, and with a contact time of 380 min [31]. The removal efficiency of Ni^{2+} ions using PGNS was 83.84% at pH 7, whereas it was 36.97% for PG (Fig. 9). The saturation time for PGNS was 170 minutes, which was shorter than that of the control group, PG, which took 200 minutes. The results suggest that PG and PGNS can effectively eliminate

the target contaminant, achieving peak removal rates of 36.97% at pH 7 (Table 3).

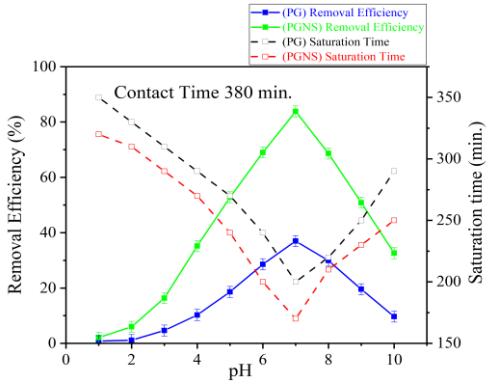

Fig. 9. Ni^{2+} removal efficiency and saturation time of PG and PGNS, error bars represent the standard deviation of triplicate measurements

Remarkably, the highest reported reduction effectiveness was 0.8%. The study demonstrates that, especially at high or low pH values, the removal efficiency is distinctly lower; at a pH value of 1, the removal efficiency was steady at this low level. Additionally, it was found that PG has a maximum solubility of 0.1 M after 350 minutes, and PGNS demonstrates effectiveness with a percentage removal efficiency of 83.34%. Nevertheless, in a highly acidic solution, the concentration reduces to 2. For the nanoparticles, the saturation time was 320 minutes at pH 1. Similar to Fe^{2+}, the removal efficiency for Ni^{2+} using PGNS was also lower at pH 10 than at pH 5. This behavior can be attributed to some extent to the formation of $Ni(OH)_2$ precipitates on the adsorbent and due to the electrostatic repulsion between the $–NH^+$ group of the adsorbent surface and the $Ni(OH)_3^-$ ions at high pH. The competition between OH^- ions and Ni^{2+} ions for the adsorption sites also resulted in low efficiency at pH 10. From this study, it is evident that the adsorption capacity of Ni^{2+} ions varies with the pH value of the solution. Moreover, the saturation time for PGNS was significantly shorter, particularly under pH 1 and seven conditions at 320 min and 170 min, respectively. The results also indicate that at high pH values, the removal effectiveness of nanoparticles is higher than that of activated carbon for both materials. Thus, in a given context, further studies are needed to investigate the effectiveness of certain materials in specific pH ranges and their ability to remove specific pollutants from the medium.

Table 2. The removal efficiency and the saturation time of Fe ions using PG and PGNS

	Fe^{2+} ions					
	Removal Efficiency (%)			Saturation Time (min.)		
	pH 1	pH 7	pH 10	pH 1	pH 7	pH 10
PG	1.92	43.71	19.68	330	180	250
PGNS	5.82	94.89	49.3	310	150	220

Table 3. The removal efficiency and the saturation time of Ni ions using PG and PGNS

	Ni^{2+} ions					
	Removal Efficiency (%)			Saturation Time (min.)		
	pH 1	pH 7	pH 10	pH 1	pH 7	pH 10
PG	1.24	40.6	20.1	340	170	250
PGNS	4.21	91.11	46.02	320	150	220

3.10. Validation models for adsorption

3.10.1 Langmuir Isotherm Analysis

The Langmuir adsorption isotherm is a cornerstone in studying the interactions between adsorbates and adsorbents within a specific system. This model effectively elucidates how molecules adhere to a surface until it reaches its saturation point, providing valuable insights into numerous adsorption mechanisms across various disciplines [32,33]. The model posits that at equilibrium, the adsorption rate of the molecule matches the desorption rate, ensuring a dynamic balance within the system. Below are Eqs. (3-7) that demonstrate the Langmuir adsorption model, along with its linear fitting for further analysis:

$$Q_e(mg/g) = (C_i - C_e) * (V/W) \quad (3)$$

$$q_{max} = 1/Intercept \quad (4)$$

$$K_L = 1/(slope * q_{max}) \quad (5)$$

$$R_L = 1/(1 + C_i * K_L) \quad (6)$$

$$Linear\ fitting: 1/q_e = 1/(K_L * C_e) + (a_L/K_L) \quad (7)$$

The term (q_e) in mg/g is a variable that evaluates the quantity of molecules bound to the adsorbent within a specific time duration. The equilibrium concentration of the solution is represented by (C_e) in mg/l, and the initial concentration of the solution is represented by (C_i) in mg/l. The variable V signifies

the volume of the heavy metal solution in litres. The relationship of the Langmuir isotherm model in the most energy-effective adsorption and the sorption equilibrium capacity is described by *W* (weight of the adsorbent material in g), q_{max} (maximum adsorption capacity in mg/g of the material), and K_L (Langmuir factor in l/mg) among other parameters. The results in Figs. 10 (a-b) clearly show the adsorption of iron ions with PG and PGNS using Langmuir's isotherm model. Additionally, Figs. 11 (a-b) depict the Langmuir isotherm plot for Nickel ion removal from the sample matrices. To be more specific, the adsorption results indicate that the isotherm data of the PGNS sample align very well with the Langmuir model, in contrast to the PG sample.

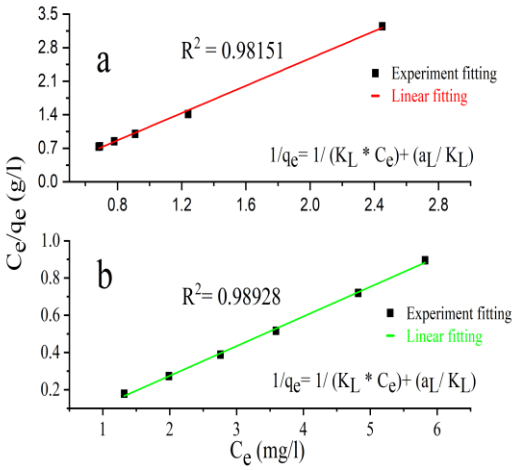

Fig. 10. Langmuir isotherm analysis for Fe^{2+} removal efficiency by a) PG, b) PGNS

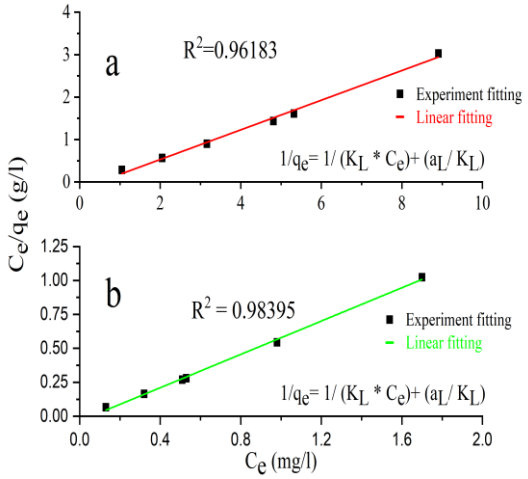

Fig. 11. Langmuir isotherm analysis for Ni^{2+} removal efficiency by a) PG, b) PGNS

3.10.2 Freundlich Isotherm Analysis

The Freundlich isotherm model is one of the most important models to model and explains molecules' multilayer and heterogeneous adsorption behavior on the adsorbent surface [34,35]. It is mathematically represented by the nonlinear fitting Eq. (8):

$$Nonlinear\ fitting\ equation: q_e = K_F * {C_e}^{1/n} \quad (8)$$

The values of K_F, known as the Freundlich constant and (*n*) equation, give information about adsorption behavior. Symbolically, K_F which is in the unit of mg/g (L/mg)1/n, shows adsorbent capacity towards the effluent, and n describes the heterogeneous surface, displaying insight into the dispersion of the molecules on the adsorbent. Its value is higher than one, suggesting that the adsorption is strong on the surface, or in other words, a higher value of n represents a more intense adsorption.

Figs. 12 (a-b) illustrate the relationship between the experimental outcomes of the adsorption of Fe^{2+} ions and the outcomes of the application of the Freundlich isotherm model. It is clearly shown that the synthetic nanoparticles have a better match with the model than the other developed samples. The results of the further analysis, as presented in Figs. 13(a-b) confirmed the correlation between nickel ion adsorption and the Freundlich model, which supports the adequacy of the proposed model for analyzing the adsorption behavior of both iron and nickel ions.

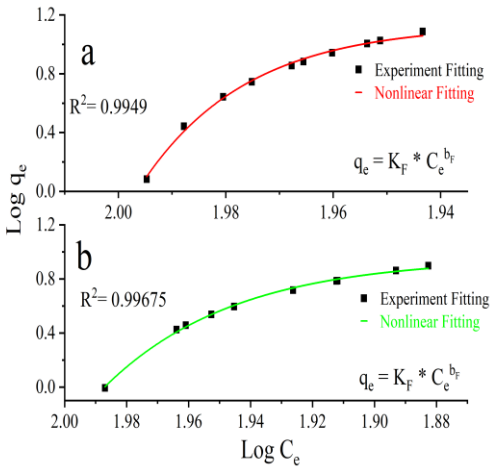

Fig. 12. Freundlich isotherm analysis for Fe^{2}+ removal efficiency by a) PG, b) PGNS

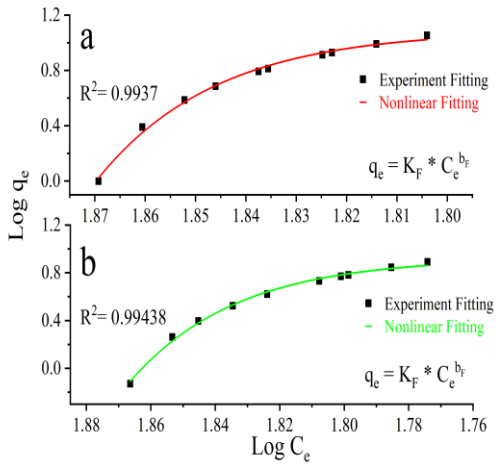

Fig. 13. Freundlich isotherm analysis for Ni^{2+} removal efficiency by a) PG, b) PGNS

4. CONCLUSION

New studies show that pomegranate peel nanostructures PGNS with diameters of 45-60 nm can be considered as bio-adsorbents for the removal of heavy metals, particularly Fe^{2+} and Ni^{2+} ions, with high efficacy. The removal efficiency of these nanostructures exceeds 83% for certain pH levels and interaction durations. PGNS exhibited more favorable characteristics compared to previously developed pomegranate peel PG adsorbents, confirming that cost-effective solutions exist for heavy metal removal from water while also mitigating agricultural waste and pollution. Treating waste containing toxic substances that threaten ecological balance and human beings is incredibly important. Nanomaterials have proven to be far more efficient than previous treatment methods due to their high and stable adsorption rate. This work reveals the role of nanomaterials in water treatment, producing contamination-free water through the adsorption and capping of metal ions in water. More work should be done regarding the industrial applications of these as-prepared high-performance nanomaterials, such as investigations into other methods of preparation and operating conditions for actual use. It is necessary to set up processes to prepare and utilize PGNS as adsorbents for achieving PGNS own-based preparation and environmental sustainability. Although this work demonstrated that pomegranate peel nanoparticles (PGNS) are an effective adsorbent for removing Fe^{2+} and Ni^{2+} ions, the adsorbent's regeneration and recovery process was not explored. Future work will investigate the effect of various eluting agents on the desorption of adsorbed metal ions, the performance of PGNS in multiple adsorption-desorption cycles, and structural and chemical changes of the adsorbent after regeneration. Such studies will help generate important information on the feasibility and economically sustainable practice of PGNS in treating real-world wastewater.

CONFLICTS OF INTEREST

The authors declare no conflict of interest.

REFERENCES

[1] K.M. Aboelghait, W.E. Abdallah, I. Abdelfattah, A.M. El-Shamy, Green synthesis of silver nanoparticles by waste of Murcott Mandarin peel as a sustainable approach for efficient heavy metal removal from metal industrial wastewater. *Separation and Purification Technology*, 347, 2024: 127609. https://doi.org/10.1016/j.seppur.2024.127609

[2] A. Ahmad, Z.U. Khan, S. Sabahat, J. Sun, N.S. Shah, Z.U. Khan, N. Muhammad, S. Mir, A. Rahim, M. Nadeem, S. Khasim, Innovations in metal oxides-biochar nanoparticles for dye removal. *Nano-Structures & Nano-Objects*, 39, 2024: 101269. https://doi.org/10.1016/j.nanoso.2024.101269

[3] O.J. Ajala, A. Khadir, J.O. Ighalo, G.C. Umenweke, Cellulose-based nano-biosorbents in water purification. *Nano-Biosorbents for Decontamination of Water, Air, and Soil Pollution*, 2022: 395-415. https://doi.org/10.1016/B978-0-323-90912-9.00017-4

[4] M. Alisher, D. Shah, M. Izquierdo, S.Ybray, Y. Sarbassov, Synergistic effects of Cl-donors on heavy metal removal during sewage sludge incineration. *Case Studies in Chemical and Environmental Engineering*, 10, 2024: 100876. https://doi.org/10.1016/j.cscee.2024.100876

[5] L. Cundari, A.L. Fanneza, N.C. Arisma, Characterization of Biosorbent from Musa acuminata balbisian peel using FTIR spectroscopy and its application to cadmium (Cd) removal: Effect of activator type, pH, and Biosorbent ratio. *CHEMICA: Jurnal Teknik Kimia*, 9(3), 2023: 142. https://doi.org/10.26555/chemica.v9i3.23992

[6] S. Das, S. Kumar, A. Kumar Mehta, M.K. Ghangrekar, Heavy metals removal by algae and usage of activated metal-enriched biomass as cathode catalyst for improving performance of photosynthetic microbial fuel cell.

Bioresource Technology, 406, 2024: 131038. https://doi.org/10.1016/j.biortech.2024.131038

[7] C. Miao, W. Huang, K. Li, Y. Yang, Highly efficient removal of adsorbed cationic dyes by dual-network chitosan-based hydrogel. *Environmental Research*, 263, 2024: 120195. https://doi.org/10.1016/j.envres.2024.120195

[8] M.A. Dheyab, N. Oladzadabbasabadi, A.A. Aziz, P.M. Khaniabadi, M.T.S. Al-ouqaili, M.S. Jameel, F.S. Braim, B. Mehrdel, M. Ghasemlou, Recent advances of plant-mediated metal nanoparticles: Synthesis, properties, and emerging applications for wastewater treatment. *Journal of Environmental Chemical Engineering*, 12(2), 2024, 112345. https://doi.org/10.1016/j.jece.2024.112345

[9] R. Divahar, T. Meenambal, J.S. Mary, P.S. Aravind Raj, S.P. Sangeetha, S.A.A. Anand, Lemon peel activated carbon: A sustainable solution for lead ion removal from E-waste bioleachate. *Sustainable Chemistry for the Environment*, 6, 2024: 100094. https://doi.org/10.1016/j.scenv.2024.100094

[10] M. El-Fahaam, M. N. Sanad, M. Farouz, Achievements and difficulties with batch and optimization investigations of heavy metal adsorptive removal utilizing enhanced biomass-based adsorption materials. *Current Nanoscience*, 21(1), 2025: 24-36. https://doi.org/10.2174/0115734137282899240102085324

[11] M. Farouz, S. El-Dek, M. ElFaham, U. Eldemerdash, Ecofriendly sustainable synthetized nano-composite for removal of heavy metals from aquatic environment. *Applied Nanoscience*, 12(5), 2022: 1585-1600. https://doi.org/10.1007/s13204-021-02331-3

[12] S. Firdaus, F. Ahmad, S. Zaidi, Preparation and characterization of biodegradable food packaging films using lemon peel pectin and chitosan incorporated with neem leaf extract and its application on apricot fruit. *International Journal of Biological Macromolecules*, 263, 2024: 130358. https://doi.org/10.1016/j.ijbiomac.2024.130358

[13] N.P.F. Gonçalves, E.F. Da Silva, L.A.C. Tarelho, J.A. Labrincha, R.M. Novais, Simultaneous removal of multiple metal(loid)s and neutralization of acid mine drainage using 3D-printed bauxite-containing geopolymers. *Journal of Hazardous Materials*, 462, 2024: 132718. https://doi.org/10.1016/j.jhazmat.2023.132718

[14] A. Gupta, A. Roy, Scope of nanomaterials in treating wastewater produced by industries. *Advancements in Bio-systems and Technologies for Wastewater Treatment. Water Science and Technology Library*, 118, 2024: 269-291. https://doi.org/10.1007/978-3-031-58331-5_14

[15] M.K. Hussain, S. Khatoon, G. Nizami, U.K. Fatma, M. Ali, B. Singh, A. Quraishi, M.A. Assiri, S. Ahamad, M. Saquib, Unleashing the power of bio-adsorbents: Efficient heavy metal removal for sustainable water purification. *Journal of Water Process Engineering*, 64, 2024: 105705. https://doi.org/10.1016/j.jwpe.2024.105705

[16] U.M. Ismail, M.S. Vohra, S.A. Onaizi, Adsorptive removal of heavy metals from aqueous solutions: Progress of adsorbents development and their effectiveness. *Environmental Research*, 251, 2024: 118562. https://doi.org/10.1016/j.envres.2024.118562

[17] O. Khan, M. Parvez, A.K. Yadav, A comparative analysis of various nanocomposites for the remediation of heavy metals from biomass liquid digestate using multi-criteria decision methods. *Biomass and Bioenergy*, 186, 2024: 107281. https://doi.org/10.1016/j.biombioe.2024.107281

[18] B. Liu, L. Zhang, K. Ning, W. Yang, Biochar with nanoparticle incorporation and pore engineering enables enhanced heavy metals removal. *Journal of Environmental Chemical Engineering*, 11(5), 2024: 111056. https://doi.org/10.1016/j.jece.2023.111056

[19] C.L. Londoño-Calderón, P. Tancredi, S. Menchaca-Nal, N.J. Francois, L.G. Pampillo, Synergistic effects in magnetically recoverable nanocomposites of CuO nanoleaves with Fe_3O_4 nanoparticles for organic dye degradation. *Next Materials*, 7, 2024: 100370. https://doi.org/10.1016/j.nxmate.2024.100370

[20] R. Meena, M.M.S. Abdullah, V. Vasanthakumar, D. Ravichandran, S. Murugesan, Green biochar-supported $ZnFe_2O_4$ composite photocatalyst derived from waste banana peel: A sustainable approach for highly efficient visible light-driven degradation of organic pollutants in wastewater. *Ionics*, 30, 2024: 5639-5650.

https://doi.org/10.1007/s11581-024-05665-4

[21] M.F. Mohamad Yusop, A.Z. Abdullah, M.A. Ahmad, Amoxicillin adsorption from aqueous solution by Cu(II) modified lemon peel based activated carbon: Mass transfer simulation, surface area prediction and F-test on isotherm and kinetic models. *Powder Technology*, 438, 2024: 119589. https://doi.org/10.1016/j.powtec.2024.119589

[22] A. Musa Jaber Al-Maliki, M. Masrournia, R. Sanavi Khoshnood, A. Beyramabadi, Dispersive micro solid-phase extraction with bimetallic Ni, Zn-MOF sorbent and gas chromatography method for Organophosphorus pesticide determination in environmental water samples. *Microchemical Journal*, 205, 2024: 111259. https://doi.org/10.1016/j.microc.2024.111259

[23] N. Mushahary, A. Sarkar, F. Basumatary, S. Brahma, B. Das, S. Basumatary, Recent developments on graphene oxide and its composite materials: From fundamentals to applications in biodiesel synthesis, adsorption, photocatalysis, supercapacitors, sensors and antimicrobial activity. *Results in Surfaces and Interfaces*, 15, 2024: 100225. https://doi.org/10.1016/j.rsurfi.2024.100225

[24] A.O. Nasser, S.L. Kareem, Removal of Congo red from aqueous solution using lemon peel-Fe_3O_4 nanocomposite adsorbent. *Biomass Conversion and Biorefinery*, 14, 2023: 23183-23193. https://doi.org/10.1007/s13399-023-04496-z

[25] B. Natarajan, P. Kannan, L. Guo, Metallic nanoparticles for visual sensing: Design, mechanism, and application. *Chinese Journal of Structural Chemistry*, 43(9), 2024: 100349. https://doi.org/10.1016/j.cjsc.2024.100349

[26] M. Radenković, J. Petrović, S. Pap, A. Kalijadis, M. Momčilović, N. Krstulovič, S. Živković, Waste biomass derived highly-porous carbon material for toxic metal removal: Optimisation, mechanisms and environmental implications. *Chemosphere*, 347, 2024: 140684. https://doi.org/10.1016/j.chemosphere.2023.140684

[27] M.N. Sanad, M. Farouz, M.M. ElFaham, Recent advancement in nano cellulose as a biomass-based adsorbent for heavy metal ions removal: A review of a sustainable waste management approach. *Advanced Engineering Letters*, 2(4), 2023: 120-142. https://doi.org/10.46793/adeletters.2023.2.4.1

[28] M.N. Sanad, S.I. El-Dek, U. Eldemerdash, M. ElFaham, Study of the adsorptive removal of (Fe^{+2}) and (Ni^{+2}) from water by synthesized magnetite/corn cobs magnetic nanocomposite. *Nano Futures*, 6, 2022: 025004. https://doi.org/10.1088/2399-1984/ac6a31

[29] N.M Sayed, S.A.H. Abo farha, Valorization of lemon peel as low-cost adsorbent for the removal of basic fuchsine and eosin dyes from aqueous solutions. *International Journal of Theoretical and Applied Research*, 2(1), 2023: 139-153. https://doi.org/10.21608/ijtar.2023.197859.1041

[30] A.M. Rajalakshmi, T. Silambarasan, R. Dhandapani, Biosorption of heavy metals from tannery effluents by using green unicellular Microalga, Tetradesmus obliquus RDRL01. *Applied Biological Research*, 24(1), 2022: 28-37. https://doi.org/10.5958/0974-4517.2022.00008.8

[31] N. Wang, M. Wang, H. Quan, S. Wang, D. Chen, Waste camellia oleifera shell-derived hierarchically porous carbon modified by Fe_3O_4 nanoparticles for capacitive removal of heavy metal ions. *Separation and Purification Technology,* 329, 2024: 125184. https://doi.org/10.1016/j.seppur.2023.125184

[32] M.N. Sanad, M. Okil, M.M. ElFaham, Fascinating physicochemical features of wasted biomass nanoscale biosorbent for heavy metal ions removal from water. *International Journal of Environmental Science and Technology*, 2025. https://doi.org/10.1007/s13762-024-06304-1

[33] H.M. Hashem, M. El-Maghrabey,R. El-Shaheny, Inclusive study of peanut shells derived activated carbon as an adsorbent for removal of lead and methylene blue from water. *Scientific Reports*, 14, 2024: 13515. https://doi.org/10.1038/s41598-024-63585-9

[34] M. S.F. Al-Hazeef, A. Aidi, L. Hecini, G. G.Hasan, J. Hu, M. Althamthami, Unveiling the efficiency of peanut shell-derived porous composite for water denitrification: Characterization, kinetic, isotherm and thermodynamic studies. *Journal of Molecular Liquids*, 410, 2024: 125668. https://doi.org/10.1016/j.molliq.2024.125668

[35] N.T. Pessôa, D.C.S. Sales, G.E.D. Nascimento, J.H.L. dos Santos, M.N. dos Santos Silva, D.C. Napoleão, J.M.Rodríguez-Díaz, M.M.M.B. Duarte, Effective adsorption of cadmium and nickel ions in mono and bicomponent systems using eco-friendly adsorbents prepared from peanut shells. *Environmental Research*, 247, 2024: 118220. https://doi.org/10.1016/j.envres.2024.118220